

Low Density 2D Superlattices Assembled via Directional DNA Bonding

Ziyi Miao^{*,[a,c]}, Cindy Y. Zheng^{*,[b,c]}, George C. Schatz^{*,[a,c]}, Byeongdu Lee,^{*,[d]} and Chad A. Mirkin^{*,[a,b,c]}

- [a] Z. Miao^{*}, Prof. C. A. Mirkin^{*}
Department of Materials Science and Engineering
Northwestern University
2220 Campus Drive, Evanston, IL 60208, USA
E-mail: chadnano@northwestern.edu
- [b] C. Y. Zheng^{*}, Prof. G. C. Schatz, Prof. C. A. Mirkin^{*}
Department of Chemistry
Northwestern University
2145 Sheridan Road, Evanston, IL 60208, USA
- [c] Z. Miao^{*}, C. Y. Zheng^{*}, G. C. Schatz, C. A. Mirkin^{*}
International Institute for Nanotechnology, Northwestern University
- [d] Dr. B. Lee
X-ray Science Division
Argonne National Laboratory
9700 South Cass Avenue, Argonne, Illinois, 60439, USA
E-mail: blee@anl.gov

+ These authors contributed equally to this work.

Supporting information for this article can be found at: doi:10.1002/anie.2021XXXXX

Abstract: It is critical to assemble nanoparticles (NPs) into superlattices with controlled symmetries and spacings on substrates for metamaterials applications, where such structural parameters dictate their properties. Here, we use DNA to assemble anisotropic NPs of three shapes - cubes, octahedra, and rhombic dodecahedra - on substrates and investigate their thermally induced reorganization into two-dimensional (2D) crystalline films. We report two new *low-density* 2D structures, including a honeycomb lattice based on octahedral NPs. The low-density lattices favoured here are not usually seen when particles are crystallized via other bottom-up assembly techniques. Furthermore, we show that, consistent with the complementary contact model, a primary driving force for crystallization is the formation of directional, face-to-face DNA bonds between neighbouring NPs and between NPs and the substrate. Our results can be used to deliberately prepare crystalline NP films with novel morphologies.

Colloidal nanoparticle (NP) superlattices (SLs) can behave as metamaterials with unique optical,^[1,2] electrical,^[3,4] and magnetic^[5] properties based on the structure-dependent interactions between the particles that comprise them. As such, researchers have devoted significant effort towards developing methods to prepare ordered assemblies of colloidal NPs with control over various structural parameters.^[1,5-8] Colloidal crystal engineering with DNA, which utilizes DNA-grafted NPs as “programmable atom equivalents” (PAEs), has arisen as a versatile method to fabricate SLs with remarkable control over lattice symmetry and spacing independent of the size, shape, and composition of the NP core.^[9-11] Indeed, this method has been used to prepare SLs in solution with over 50 distinct symmetries, some displaying interesting optical properties, including birefringence,^[12] unnaturally high refractive indices,^[2] and directional emission.^[13] Furthermore, thin-films of spherical PAEs have been assembled on substrates with control over crystal thickness and orientation,^[14,15] opening the door to the measurement of their optical^[16] and mechanical properties^[17] as well as their integration into devices.^[18] Although the feasibility of this surface-bound growth technique has been demonstrated

using spherical PAEs, anisotropic PAEs have not yet been explored in this context, and these particles offer an additional degree of structural control in assembly due to shape-induced directional bonding.^[1,19,20] In addition, films of anisotropic plasmonic NPs may find even greater applicability in optical devices compared to their spherical counterparts due to the strong shape- and size-dependent scattering of the individual NPs^[21,22] and the extreme electric field confinement between neighbouring NPs.^[16,23,24]

In this work, we investigate the assembly of complementary systems of Au PAEs with three polyhedral cores – cubes, octahedra, and rhombic dodecahedra (RD) – into thin-films on DNA-functionalized substrates. We predicted that, in accordance with previous studies and the complementary contact model (CCM)^[9] involving the DNA-mediated assembly of polyhedral PAEs in solution, these PAEs would thermally reorganize into SL films with symmetries that maximize the face-to-face interactions between particles.^[25] Moreover, we expected the bottom-most layer of NPs to orient with their facets parallel to the flat substrate in order to maximize DNA binding, as predicted by the CCM.^[9] Because SL orientations resulting from large NP facets parallel to the substrate do not necessarily expose the closest-packed planes of a specific system, we hypothesized that this approach could allow for the assembly of open 2D lattices.

Indeed, although we found that cubic PAEs form close-packed films, we saw that RD PAEs, which form face centered-cubic (FCC) lattices in solution with {111} closest-packed planes, rearrange into 2D films on surfaces with a rhombic symmetry (corresponding to the open {110} planes of an FCC lattice). Furthermore, octahedral PAEs, which form body-centered cubic (BCC) lattices in solution with {110} closest-packed planes, rearrange into 2D films on surfaces with a honeycomb symmetry, corresponding to the open {111} planes of a BCC lattice. Neither of these unusual 2D lattices have been obtained by conventional entropy-driven NP crystallization, in which the formation of close-packed arrangements is favored.^[7,26] Open structures are desirable in applications, spanning sensing to nanophotonics.^[8,27] Taken together, our results provide fundamental insight into the growth of of PAE SLs on substrates and demonstrate the

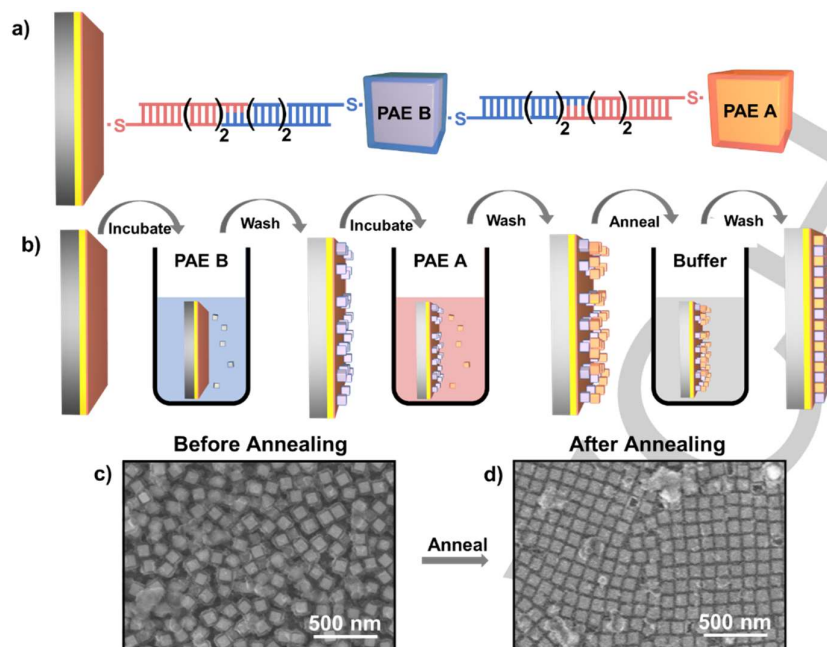


Figure 1. a) Schematic of the DNA design. A hetero-complementary DNA system is used. PAE A and the substrate are functionalized with A-type DNA (red), while particle B is functionalized with B-type DNA (blue). The stacked configuration is observed prior to annealing. b) Schematic of the assembly process. c) SEM image of an unannealed two-layer assembly. d) SEM image of the thermally annealed crystalline PAE monolayer thin-film.

capability of colloidal crystal engineering with DNA for preparing optical metamaterials with unusual, but potentially useful properties and functions.

To assemble films with controlled thicknesses, we utilized a binary system of “A” and “B”-type polyhedral PAEs, where DNA A and B are comprised of complementary “sticky ends” (Figure 1a). First, we grew two-layer amorphous films by functionalizing a Au-coated wafer with A-type DNA and then assembling B-type PAEs followed by A-type PAEs (Figure 1b,c). Next, the film was annealed just below the melting temperature of aggregates of PAE A and PAE B (T_m), allowing for its rearrangement into an ordered 2D, single-layer SL (Figure 1d). Finally, the samples were transferred into the solid state by embedding them in a silica matrix,^[28] and scanning electron microscopy (SEM) and grazing-incidence small-angle X-ray scattering (GISAXS) were performed. Large-area SEM images show that these films were grown in high uniformity over macroscopic areas (Figure S22). Importantly, although the resulting annealed films appear as monolayers in top-down SEM images, depending on the system, the A and B-type particles could be situated at different heights due to their distinct shape-driven bonding characteristics.

Films were formed with the three different-shaped PAEs mentioned above (Figure 2). We first examined a system consisting of cubic PAEs, which forms a simple cubic (SC) lattice with $\{100\}$ closest-packed planes in solution.^[24] Because cubic NPs are bound by $\{100\}$ facets, when assembled on DNA-functionalized substrates, they should orient with the $\langle 100 \rangle$ direction perpendicular to the surface to maximize particle-substrate face-to-face binding. Indeed, SEM images of an assembly of 80-nm cubic NPs revealed a 2D square lattice with individual NPs oriented in the $\langle 100 \rangle$ direction (Figure 2a). This film is equivalent to the $\{100\}$ planes of a SC lattice. Because we utilized a binary system of cubic PAEs, where B-type PAEs are able to hybridize with the DNA on the substrate, and where A-type

PAEs are not, we predicted that neighboring A- and B-type PAEs would be situated at different heights in these structures. However, SEM images at 30° and 90° tilt angles (Figures 2c, S15a) as well as GISAXS scattering patterns (Figure 2d) suggest that both A- and B-type cubic PAEs lie within the same plane, post-annealing. This indicates that interparticle face-to-face hybridization interactions overcome the repulsive interactions between the NP and substrate, which are functionalized with the same DNA. As a result, the binary cubic system forms a *high density* film that exposes its closest-packed (100) plane even though only B-type PAEs form DNA bonds with the substrate that is functionalized with A-type DNA. SEM images (Table S2) and a fit of GISAXS data (Figure S10a) confirm that the films indeed adopt a 2D square symmetry with a lattice constant of 126 nm.

Next, we studied a binary octahedral system using NPs with edge lengths of 80 nm. The assembly of octahedral PAEs and their spherical counterparts can be directly compared, since in solution both systems form BCC SLs with RD Wulff shapes that expose their $\{110\}$ closest-packed planes.^[25,28] Among the low-index planes in a BCC lattice, the packing density goes as $\{110\} > \{100\} > \{111\}$.^[29] When assembled onto a DNA-functionalized substrate, a binary system of spherical PAEs forms a film oriented in the $\langle 100 \rangle$ direction.^[14] Importantly, this system adopts a non-close-packed orientation to maximize complementary NP-substrate bonds. However, unlike with the spherical system, octahedral PAEs reorganize into buckled honeycomb structures on substrates after assembly and annealing. This buckled honeycomb structure is equivalent to the $\{111\}$ plane of a BCC lattice, as evidenced by SEM and GISAXS (Figure 2i-k, Table S2). Specifically, the GISAXS diffraction pattern can be assigned to a 2D hexagonal structure with two NPs per lattice point (Figure S17b), together comprising a honeycomb structure with a lattice constant of 165 nm. In this structure, each octahedral NP core is oriented in the $\langle 111 \rangle$ direction, and the resultant film exposes the

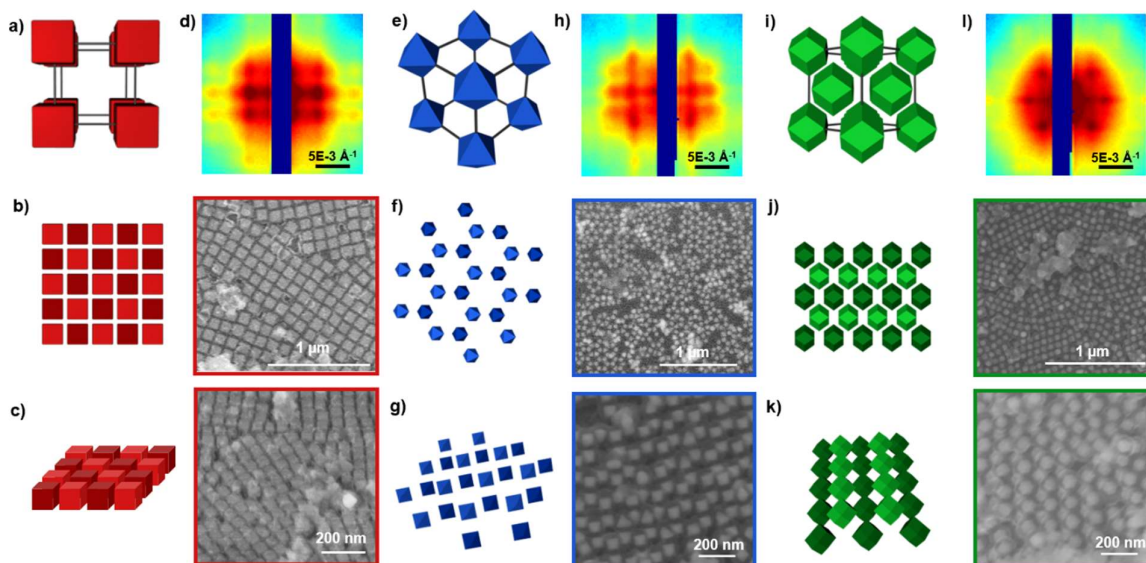


Figure 2. NP films. a,e,i) Schematics of the unit cells of cubic, octahedral, and RD PAE SLs rotated to match the orientation of the resulting 2D films. b,f,j) Schematics and corresponding SEM images of the resulting 2D films. Square, honeycomb, and rhombic symmetries were observed in films consisting of cubic, octahedral, and RD PAEs, respectively. c,g,k) Schematics and corresponding SEM images taken at a 30° tilt angle showing the height difference between A and B-type PAEs in each structure. d,h,l) GISAXS scattering patterns from the samples in b,f, and j, respectively.

{111} plane of a BCC SL. Notably, although 2D colloidal honeycomb SLs have been assembled using sub-10-nm NPs sub-10-nm NPs^[6,30] and micron-sized particles,^[31] this is the first time they have been prepared using NPs in the ~100-nm size range, which is most relevant for plasmonics and metamaterials. In fact, lithographically patterned honeycomb SLs at this length scale behave as the photonic counterpart of graphene, exhibiting extraordinary phenomena including Dirac-like plasmons^[32–34] and complete photonic bandgaps.^[35,36]

Furthermore, this result elucidates the effect of shape-induced directionality on thin-film orientation. The drive of the system to maximize face-to-face interactions in polyhedral PAE systems affects the resulting SL orientation. Our observations are explained by a simple surface energy model, which demonstrates that when face-to-face NP-substrate interactions are present, the surface energy of the open {111} plane becomes lower than that of the closest-packed {110} plane (see Supporting Information). We also attempted to assemble films of octahedral PAEs with more than two layers, but interestingly, the resulting SLs were mostly amorphous (Figure S21). SEM images taken at a 90° tilt angle, post-annealing, (Figure S15b) revealed that A-type octahedral PAEs were situated at heights ~25% higher than expected based on a measurement of the bulk BCC system (Table S2). This result is likely due to the repulsion of the A-type octahedral PAEs with the A-type substrate-bound DNA. This distortion of the 3D lattice likely explains why multi-layer crystalline films did not form.

The role of particle shape was further investigated using RD PAEs with edge lengths of 51 nm, which assemble into an FCC lattice with {111} closest-packed planes in solution.^[25] A 2D rhombic SL with a lattice constant of 113 nm resulted from the assembly and annealing of these particles onto a DNA-functionalized substrate, as determined by GISAXS. This architecture can be matched with the {110} planes of an FCC lattice (Figure 2k). Furthermore, SEM images taken at a 90° tilt angle revealed that the height difference between the A- and B-

type PAEs matches closely with that of an ideal FCC lattice (Figure S15c and Table S2). Similar to the octahedral and cubic systems, individual RD PAEs are oriented with a facet parallel to the surface, in the <110> direction in this case. As was seen with the octahedral films, this structure is derived from the least dense of the three low-index planes of the corresponding 3D lattice.

To better understand the reorganization process that occurs in these systems, we studied assembly using various annealing temperatures. For example, we annealed two-layer octahedral PAE films for 4 hours at multiple temperatures below the T_m of the aggregates of octahedral PAEs A and B (47 °C, Figure 3c) and characterized the resulting films using SEM and GISAXS

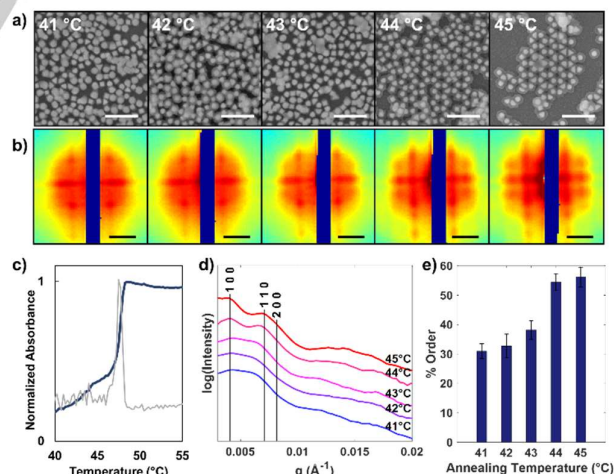


Figure 3. Assemblies of octahedral PAEs as a function of annealing temperature. a) SEM images of the assemblies at temperatures between 41 and 45 °C. Scale bars are 500 nm. b) Corresponding 2D GISAXS diffraction spectra for the films in a). Scale bars are $5\text{E}-3 \text{ \AA}^{-1}$. c) UV-vis spectroscopy of octahedral PAE aggregates in solution as it is heated. The sharp increase in absorbance at 47 °C indicates that the melting temperature (T_m) has been reached. The first derivative of the absorbance data is plotted in gray and is used to accurately determine T_m . d) 1D linecuts of the GISAXS spectra in b) taken at $q_z = 0$. e) Percent order as a function of annealing temperature.

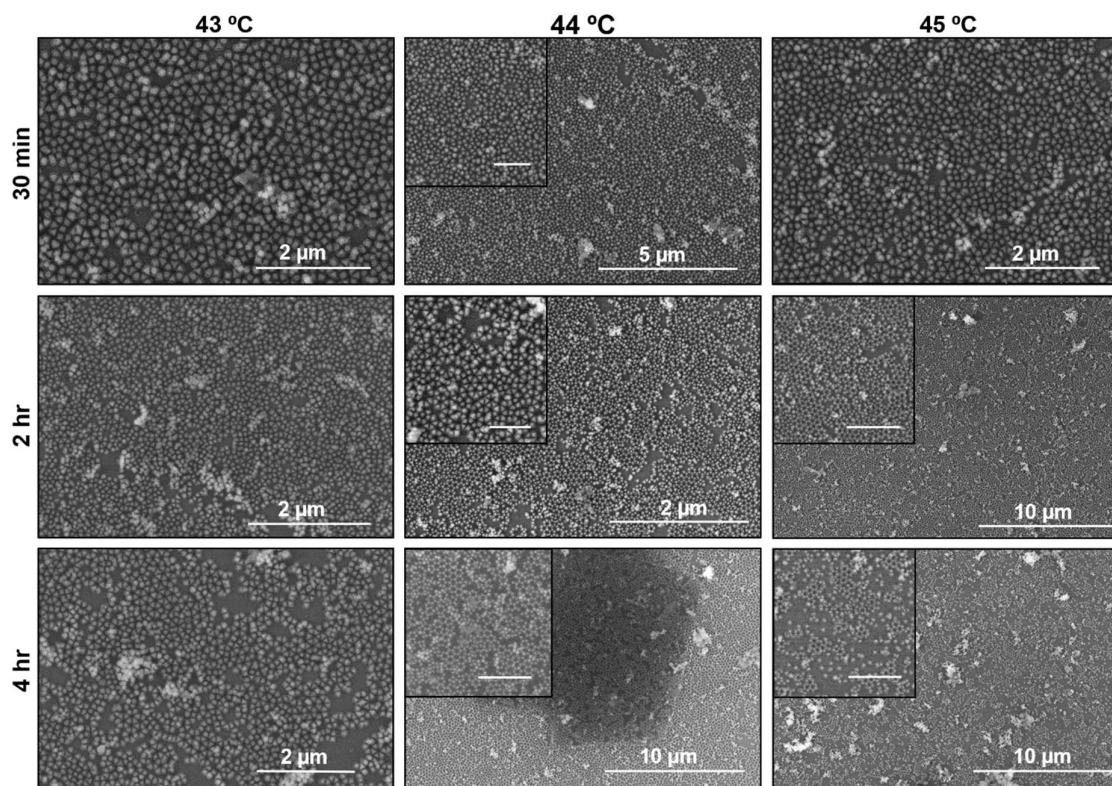


Figure 4. Large-area SEM images of two-layer octahedral PAE films grown on mono-functionalized substrates annealed at 43 °C, 44 °C, and 45 °C for 30 min, 2 hr, or 4 hr as indicated. Films annealed at 44 °C for 4 hr exhibit both high order and high coverage. Substrate annealing at 45 °C for 2 hr produces qualitatively similar results, while annealing at 45 °C for 4 hr results in films with high percent order, but lower coverage. Scale bars in insets are 2 μm .

(Figure 3). The SEM images indicate that the octahedral PAEs form mostly amorphous films at temperatures far below T_m but gradually develop a honeycomb structure with increasing crystallinity as the annealing temperature increases toward T_m . At temperatures just below T_m (44 °C), the films are comprised of a honeycomb structure with nearly 100% purity, but with lower surface coverage due to the significant melting of the PAEs from the substrate (Figures 3a, 4). Large-area SEM images (Figure 4) show that highly ordered films can be grown, while maintaining high surface coverage, by annealing at 44 °C, three degrees below T_m , for 4 hours. In addition, qualitatively similar results can be obtained by annealing at 45 °C for 2 hours. 2D GISAXS patterns further elucidate this trend; the diffraction spots sharpen as the temperature increases up to T_m (Figure 3b). 1D linecuts taken horizontally at $q_z = 0$ show the appearance of additional resolved peaks, indexed to a honeycomb structure (Figure S10b), indicating the emergence of long-range order (Figure 3d). Furthermore, SEM images were quantitatively analyzed using a homebuilt MATLAB script, and it was confirmed that, as temperature increases, percent order increases (Figure 3e). Similar trends were observed for cubic (Figures S11, S18) and RD (Figures S12, S19) films, indicating that selecting an annealing temperature near T_m results in the highest quality films with both optimized percent order and substrate coverage.

The orientation of thin-films grown using DNA-mediated assembly can be altered by modifying the substrate-bound DNA,^[14] a property unique to this system. In addition to substrates functionalized with A-DNA, we also studied the assembly of PAE films on bi-functionalized substrates with a 1:1 ratio of A:B DNA.

In the spherical BCC system, films with $\langle 100 \rangle$ orientation and the closest-packed $\langle 110 \rangle$ orientation are obtained when mono-functionalized and bi-functionalized substrates are utilized, respectively.^[14] However, for polyhedral PAEs, both SEM and GISAXS characterization indicate that the symmetries and orientations of the films assembled on bi-functionalized substrates are the same as those assembled on mono-functionalized ones (cubic PAEs form a square lattice, RD PAEs form a rhombic lattice, and octahedral PAEs form a honeycomb lattice, Figure S14), again demonstrating the influence of directional binding. Both octahedral and RD films exhibited slight distortions in lattice constants and bond angles, as the second layer of A-PAEs can also form DNA bonds with the bi-functionalized substrate (see Supporting Information).

In conclusion, we have utilized DNA to assemble crystalline thin-films comprised of polyhedral NPs and studied their reorganization as a function of NP core shape, annealing conditions, and substrate functionalization. In contrast with spherical PAEs, polyhedral PAEs form directional bonds that maximize NP-NP and NP-substrate face-to-face interactions, resulting, in certain cases, in more open crystallographic planes. The results demonstrate the importance of PAE shape on the formation of SLs on substrates and provide guidelines on how to predictably prepare desired structures by judicious choice of NP core and substrate functionalization. This additional level of control over PAE thin-film growth and the ability to access higher energy, open crystallographic planes, could aid the discovery of emerging properties from the collective optical, electrical, and magnetic responses of NPs.

Acknowledgements

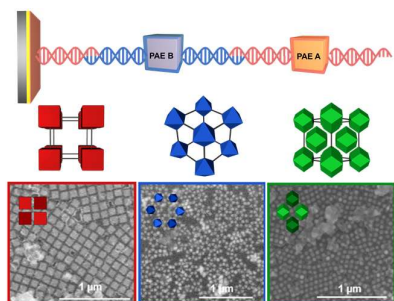
This material is based upon work supported by the Air Force Office of Scientific Research under awards FA9550-17-1-0348 (superlattice assembly) and FA9550-16-1-0150 (SAXS experiments); the Sherman Fairchild Foundation, Inc (nanoparticle synthesis); the Center for Bio-Inspired Energy Science, an Energy Frontier Research Center funded by the U.S. Department of Energy, Office of Science, Basic Energy Sciences under award DE-SC0000989 (computational studies); and the Air Force Research Laboratory under agreement FA8650-15-2-5518 (SEM characterization). The U.S. Government is authorized to reproduce and distribute reprints for Governmental purposes notwithstanding any copyright notation thereon. The views and conclusions contained herein are those of the authors and should not be interpreted as necessarily representing the official policies or endorsements, either expressed or implied, of Air Force Research Laboratory or the U.S. Government. This research used resources of the APS, a U.S. Department of Energy (DOE) Office of Science User Facility operated for the DOE Office of Science by Argonne National Laboratory under Contract No. DE-AC02-06CH11357. The authors would like to thank Dr. Xiaobing Zuo for his assistance with the GISAXS experiments. This work made use of the EPIC facility of Northwestern University's NUANCE Center, which receives support from the Soft and Hybrid Nanotechnology Experimental (SHyNE) Resource (NSF ECCS-1542205); the MRSEC program (NSF DMR-1121262) at the Materials Research Center; the International Institute for Nanotechnology (IIN) and the State of Illinois, through the IIN.

Conflict of Interest

The authors declare no conflict of interest.

Keywords: nanoparticles • DNA • colloidal crystals • nanoparticle superlattice • small angle X-ray scattering

- [1] A. Tao, P. Sinsermsuksakul, P. Yang, *Nat. Nanotechnol.* **2007**, *2*, 435.
- [2] S. Kim, C. Y. Zheng, G. C. Schatz, K. Aydin, K. H. Kim, C. A. Mirkin, *Nano Lett.* **2020**, *20*, 8096.
- [3] D. K. Kim, Y. Lai, B. T. Diroll, C. B. Murray, C. R. Kagan, *Nat. Commun.* **2012**, *3*, 1216.
- [4] M. Cargnello, A. C. Johnston-Peck, B. T. Diroll, E. Wong, B. Datta, D. Damodhar, V. V. T. Doan-Nguyen, A. A. Herzog, C. R. Kagan, C. B. Murray, *Nature* **2015**, *524*, 450.
- [5] J. Cheon, J. Il Park, J. S. Choi, Y. W. Jun, S. Kim, M. G. Kim, Y. M. Kim, Y. J. Kim, *Proc. Natl. Acad. Sci. U. S. A.* **2006**, *103*, 3023.
- [6] X. Wu, J. Chen, L. Xie, J. Li, J. Shi, S. Luo, X. Zhao, K. Deng, D. He, J. He, J. Luo, Z. Wang, Z. Quan, *Small* **2019**, *15*, 1901304.
- [7] E. V. Shevchenko, D. V. Talapin, N. A. Kotov, S. O'Brien, C. B. Murray, *Nature* **2006**, *439*, 55.
- [8] T. Udayabhaskararao, T. Altantzis, L. Houben, M. Coronado-Puchau, J. Langer, R. Popovitz-Biro, L. M. Liz-Marzán, L. Vuković, P. Král, S. Bals, R. Klajn, *Science* **2017**, *358*, 514.
- [9] C. R. Laramy, M. N. O'Brien, C. A. Mirkin, *Nat. Rev. Mater.* **2019**, *4*, 201.
- [10] C. A. Mirkin, R. L. Letsinger, R. C. Mucic, J. J. Storhoff, *Nature* **1996**, *382*, 607.
- [11] S. Y. Park, A. K. R. Lytton-Jean, B. Lee, S. Weigand, G. C. Schatz, C. A. Mirkin, *Nature* **2008**, *451*, 553.
- [12] M. B. Ross, M. G. Blaber, G. C. Schatz, *Nat. Commun.* **2014**, *5*, 4090.
- [13] D. J. Park, J. C. Ku, L. Sun, C. M. Lethiec, N. P. Stern, G. C. Schatz, C. A. Mirkin, *Proc. Natl. Acad. Sci. U. S. A.* **2017**, *114*, 457.
- [14] A. J. Senesi, D. J. Eichelsdoerfer, R. J. Macfarlane, M. R. Jones, E. Auyeung, B. Lee, C. A. Mirkin, *Angew. Chem. Intl. Ed.* **2013**, *52*, 6624.
- [15] L. Z. Zornberg, P. A. Gabrys, R. J. Macfarlane, *Nano Lett.* **2019**, *19*, 8074.
- [16] C. Y. Zheng, E. Palacios, W. Zhou, W. Hadibrata, L. Sun, Z. Huang, G. C. Schatz, K. Aydin, C. A. Mirkin, *Adv. Mater.* **2019**, *31*, 1904448.
- [17] D. J. Lewis, D. J. D. Carter, R. J. Macfarlane, *J. Am. Chem. Soc.* **2020**, *142*, 19181.
- [18] W. Zhou, Z. Liu, Z. Huang, H. Lin, D. Samanta, Q. Y. Lin, K. Aydin, C. A. Mirkin, *Proc. Natl. Acad. Sci. U. S. A.* **2020**, *117*, 21052.
- [19] C. W. Liao, Y. S. Lin, K. Chanda, Y. F. Song, M. H. Huang, *J. Am. Chem. Soc.* **2013**, *135*, 2684.
- [20] M. R. Jones, R. J. MacFarlane, B. Lee, J. Zhang, K. L. Young, A. J. Senesi, C. A. Mirkin, *Nat. Mater.* **2010**, *9*, 913.
- [21] J. Olson, S. Dominguez-Medina, A. Hoggard, L. Y. Wang, W. S. Chang, S. Link, *Chem. Soc. Rev.* **2015**, *44*, 40.
- [22] Z. Zhang, Z. Chen, C. Qu, L. Chen, *Langmuir* **2014**, *30*, 3625.
- [23] B. Gao, G. Arya, A. R. Tao, *Nat. Nanotechnol.* **2012**, *7*, 433.
- [24] N. A. Hatab, C. H. Hsueh, A. L. Gaddis, S. T. Retterer, J. H. Li, G. Eres, Z. Zhang, B. Gu, *Nano Lett.* **2010**, *10*, 4952.
- [25] M. N. O'Brien, H. X. Lin, M. Girard, M. Olvera de la Cruz, C. A. Mirkin, *J. Am. Chem. Soc.* **2016**, *138*, 14562.
- [26] A. Dong, X. Ye, J. Chen, C. B. Murray, *Nano Lett.* **2011**, *11*, 1804.
- [27] Y. Plotnik, M. C. Rechtsman, D. Song, M. Heinrich, J. M. Zeuner, S. Nolte, Y. Lumer, N. Malkova, J. Xu, A. Szameit, Z. Chen, M. Segev, *Nat. Mater.* **2014**, *13*, 57.
- [28] E. Auyeung, T. I. N. G. Li, A. J. Senesi, A. L. Schmucker, B. C. Pals, M. Olvera de la Cruz, C. A. Mirkin, *Nature* **2014**, *505*, 73.
- [29] Q. Fan, *J. Appl. Crystallogr.* **2016**, *49*, 1454.
- [30] M. P. Boneschanscher, W. H. Evers, J. J. Geuchies, T. Altantzis, B. Goris, F. T. Rabouw, S. A. P. van Rossum, H. S. J. van der Zant, L. D. A. Siebbeles, G. Van Tendeloo, I. Swart, J. Hilhorst, A. V. Petukhov, S. Bals, D. Vanmaekelbergh, *Science* **2014**, *344*, 1377.
- [31] F. Grillo, M. A. Fernandez-Rodriguez, M. N. Antonopoulou, D. Gerber, L. Isa, *Nature* **2020**, *582*, 219.
- [32] G. Weick, C. Woollacott, W. L. Barnes, O. Hess, E. Mariani, *Phys. Rev. Lett.* **2013**, *110*, 106801.
- [33] D. Han, Y. Lai, J. Zi, Z. Q. Zhang, C. T. Chan, *Phys. Rev. Lett.* **2009**, *102*, 123904.
- [34] S. Wang, D. Scarabelli, L. Du, Y. Y. Kuznetsova, L. N. Pfeiffer, K. W. West, G. C. Gardner, M. J. Manfra, V. Pellegrini, S. J. Wind, A. Pinczuk, *Nat. Nanotechnol.* **2018**, *13*, 29.
- [35] A. D. Snelnik, M. V. Rybin, S. Y. Lukashenko, M. F. Limonov, K. B. Samusev, *Phys. Rev. A* **2017**, *95*, 063837.
- [36] M. Polini, F. Guinea, M. Lewenstein, H. C. Manoharan, V. Pellegrini, *Nat. Nanotechnol.* **2013**, *8*, 625.

Table of Contents

Cubic, octahedral, and rhombic dodecahedral (RD) nanoparticle (NP) films are assembled on substrates using DNA. Octahedral and RD films rearrange into novel low-density 2D structures, which are difficult to access using other methods for assembling NPs into superlattices.